Chapter 1 Introduction and Literature Survey

1.1 Introduction

Graphene has attracted great attention owing to its extraordinary properties, including high carrier mobility, electrical conductivity, Young's modulus, thermal conductivity, mechanical strength and flexibility. However, the zero bandgap and semi-metallicity, limits its applications in optoelectronic devices [1-3]. Hence, it's imperative to explore other two-dimensional (2D) materials that possess an energy bandgap. After graphene, transition metal dichalcogenides (TMDs) have emerged as a predominant focus in research. Among the family of 2D TMDs, molybdenum disulfide (MoS_2), an inorganic compound, is one of the typical representative members with excellent physical, chemical and electronic properties, highly promising for future applications in advanced electronic and optoelectronic devices. It seems to resolve numerous challenges encountered by prior devices. Single-layered MoS_2 exhibits distinct properties that differ from its bulk structures. It has a significant bandgap that undergoes a transition from an indirect to direct bandgap (~1.8 eV) in thinner structures as a result of quantum confinement, showing strong photoluminescence and electroluminescence. It shows remarkable mechanical properties due to its strong covalent bonds and great elasticity [3]. It is chemically and thermally stable, transparent and flexible with good electrical and transport properties, making them excellent candidate in the field of electronic and optoelectronic applications [4]. The high carrier mobility and optical transparency makes it suitable for crafting ultra-broadband photodetectors [5]. The presence of covalent bonds between molybdenum and sulfur, and the van der Waals forces holding the layers together, makes MoS_2 particularly well-suited for gas sensing applications [6]. Apart from its various applications in device fabrication, MoS_2 shows easier and simpler ways of synthesis with

higher production yield and lower cost. In this chapter, we will be discussing all about MoS_2, like its structure, different synthesis methods, properties and applications.

1.2 Molybdenum Disulfide (MoS_2)

The large family of TMD compounds have molecular formula MX_2, where 'M' comprises of transition metals such as molybdenum, titanium, vanadium, chromium, etc. from group 4 to 10 and 'X' comprises of chalcogens from group 16 (S, Se, and Te), offering over 40 distinct combinations of elements, as shown in **Figure 1.1**. Basically, 2D TMDs are sandwich compounds of a layer of transition metal and two chalcogen atoms. In MoS_2, Mo is positive tetravalent and S is negative bivalent. Single layer of MoS_2 is three atoms thick having two hexagonal planes of S atoms parted by the plane of Mo atoms with strong covalent bond within each layer and thickness of ~0.65 nm. Bulk MoS_2 is formed from the layer-by-layer stacking of monolayers MoS_2 on top of one another through weak van der Waals interaction.

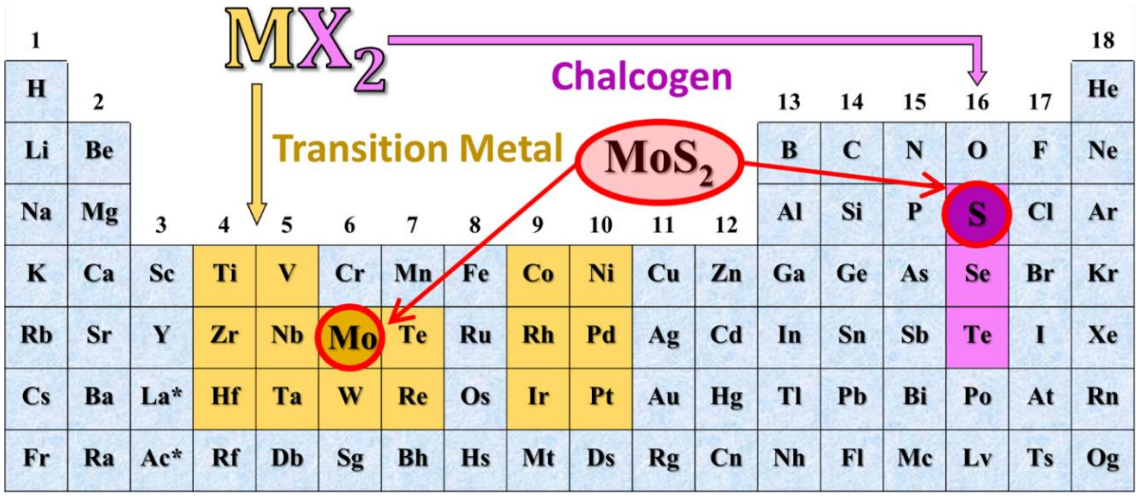

Figure 1.1 *Periodic table showing transition metal and chalcogen elements [7].*

1.3 Structure of MoS_2

MoS_2 possesses graphene like layered structure with the repeat unit X-M-X. Based on the stacking of this repeat unit along the c-axis, MoS_2 exhibits three different polytypes: 1T, 2H and 3R, with the point group D_{6d}, D_{6h} and C_{3v}, respectively. Here the first digit represents

the layer number and the second alphabet shows the crystallographic structure i.e. T for trigonal, H for hexagonal and R for rhombohedral structure. Every molybdenum (Mo) atom resides within the symmetry plane of a triangular prism, forming covalent bonds with six sulfur atoms. Simultaneously, each sulfur atom is commonly shared by three molybdenum atoms in this configuration. The 2H phase (trigonal prismatic coordination) exhibits hexagonal symmetry having two S-Mo-S layers per repeat unit while 3R phase (trigonal prismatic coordination) features rhombohedral symmetry having three S-Mo-S layers per repeat unit. In 1T phase (octahedral coordination), the upper triangle is the inversion of the bottom triangle and shows tetragonal symmetry having one S-Mo-S layer per repeat unit. The 1T and 3R phases are the metastable structures showing conductive characteristics while 2H phase is stable semiconducting structure with bandgap in the range 1.23 to 1.88 eV. The 1T phase significantly improves the charge transfer efficiency making them suitable for energy applications like supercapacitors and batteries, while the 2H-phase serves application in semiconductor-based electronic and optoelectronic devices as well as in other energy-related applications. The schematic showing the structures of different polytypes of MoS_2 is illustrated in **Figure 1.2**.

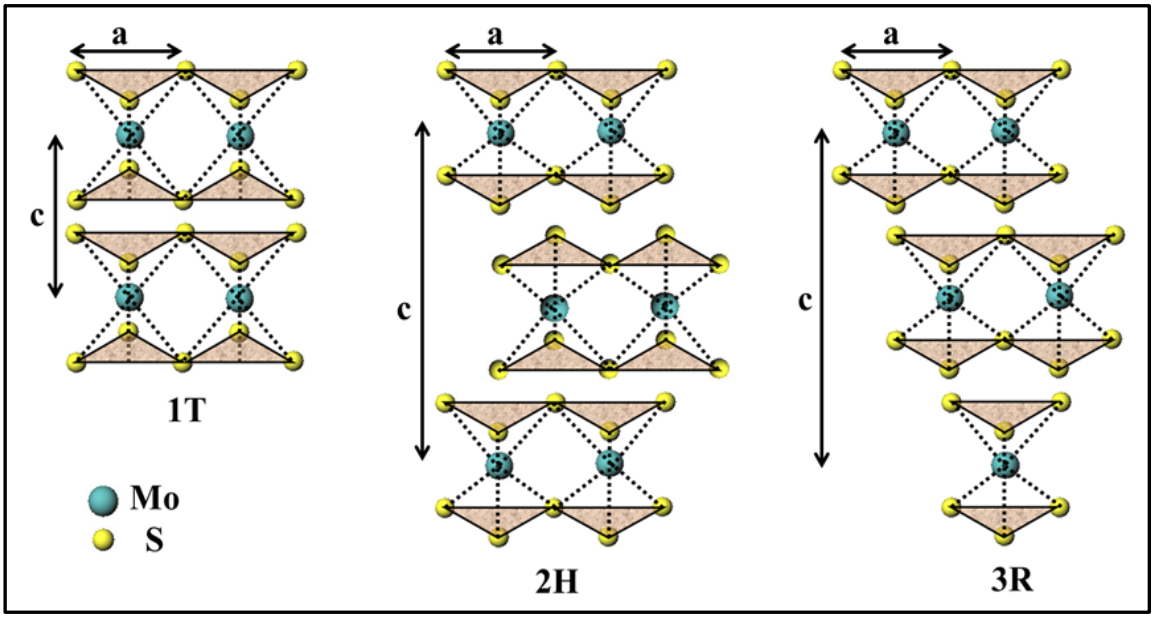

Figure 1.2 *Schematic diagram showing the different polytypes of MoS_2 [8].*

1.4 Synthesis of MoS_2

Different morphologies of MoS_2 like quantum dot, nanoplatelets, nanorods, nanowires, nanosheets, nanoribbons, nanoflakes and nanoflowers can be obtained using different synthesis techniques. Modifications in synthesis route can yield high-quality, uniform and large area MoS_2 with controlled thickness. Synthesis of MoS_2 is mainly categorized based on two approaches: top-down and bottom-up approaches. The former approach includes methods like mechanical exfoliation, liquid phase exfoliation and lithium-ion intercalation, while the bottom-up approach includes methods like physical vapour deposition, chemical vapor deposition (CVD) (thermal and plasma enhanced) and solution-based process. Here, most frequently used methods have been discussed in brief.

1.4.1 Top-Down Methods

In this method, the crafting of the 2D layered bulk nanomaterials into monolayer or few layers is accomplished through physical or chemical processes. The physical process involves exfoliating the layered structures using either the mechanical force or ultrasonic wave, while the chemical processes involve solution-based techniques such as ion exchange, heat treatment, and more. The detailed description of each of these processes are given below.

1.4.1.1 Mechanical Exfoliation

The Scotch tape exfoliation method is considered as the representative mechanical exfoliation method. In this technique, the nanosheets are detached from their bulk layered crystals through the application of mechanical force, and it works on the mechanism of weakening the van der Waals interaction present between layers utilizing adhesive scotch tape. Then, these cleaved nanosheets are transferred onto the required substrate. Once the scotch tape is removed, single to few-layer nanosheets remains over the substrate. This method is commonly known as the Scotch-tape method and was originated from Novoselov's work in

2004 by detaching a single graphene layer from graphite [9]. Subsequently, this approach was applied to 2D TMD nanomaterials like MoS_2, $MoSe_2$, $MoTe_2$, WS_2, WSe_2, TiS_2, TaS_2, ReS_2, $TaSe_2$, $NbSe_2$, etc. [10-12]. This method is recognized for its simplicity, cleanliness and cost-effectiveness in obtaining highly crystalline nanosheets but lacks scalability, is time-consuming and lacks precise control over the nanosheet thickness. To address this issue of randomness in layer thickness, nanomechanical cleavage technique was developed. In this method, a sharp tungsten tip (~10 nm) is attached to a piezoelectric motor and made contact with the crystalline edges of bulk MoS_2 for the selective layer number cleavage [13]. The MoS_2 crystal is hooked up on a support with an edge-on orientation. After contact, the tip is bend at an angle so that monolayer gets attached to the probe. By moving the tip away, the flake gets stretched and are separated from the crystal.

1.4.1.2 Liquid Phase Exfoliation

Liquid phase exfoliation method starts with bulk MoS_2, yielding flakes with random shapes, sizes and layer number, suitable for large scale production of nanomaterials. This method involves mechanical exfoliation through techniques like sonication, shearing, stirring, grinding, and bubbling. These techniques provide mechanical forces to the solvent to overcome the weak van der Waals interaction between the layers of the material. In this technique, the bulk layered material, often in powder form, are dissolved in a suitable solvent like dimethylformamide and N-methyl-2-pyrrolidone. The choice of solvent is critical, as it affects the exfoliation efficiency and dispersion stability. The solvent must have surface tension that closely matches with the material's surface energy. The solvent's intercalation between the layers weakens the van der Waals interaction of the layered material, facilitating the separation of layers. Next, the mixture undergoes mechanical or ultrasonic agitation, imparting energy to overcome the interlayer forces, resulting in the exfoliation of the layered material into nanosheets dispersed within the solvent. The process duration, solvent type, and energy input

play crucial roles in determining the quality, size, and yield of the exfoliated nanomaterials. Coleman *et al.* applied this process for the synthesis of MoS_2, $MoSe_2$, $MoTe_2$, WS_2, $TaSe_2$, $NbSe_2$, $NiTe_2$, BN and Bi_2Te_3 [14]. The advantages of this technique is its simplicity, scalability and capability to produce high-quality 2D nanomaterials without complex synthesis techniques. Despite its advantages, challenges persist in controlling the size distribution, yield and quality of the exfoliated nanomaterials.

1.4.1.3 Lithium Ion Intercalation

In the ion intercalation process, the cations such as Li^+, K^+, Na^+, etc. intercalate between layers and decreases the interlayer van der Waals interaction within the bulk crystal. Often, these intercalated ions react with water, generating hydrogen gas that helps in separating adjacent layers. Li^+ ion is preferred due to its high mobility and reduction potential. The N-Butyl lithium serves as the lithiation agent and hexane as the solvent in lithium intercalation method. Monolayer WS_2, MoS_2 and $MoSe_2$ have been achieved through lithium intercalation [15]. However, incomplete insertion of lithium ion results in low yield while its over-intercalation leads to Li_2S formation. To regulate the intercalation process, Zeng *et al.* designed the electrochemical ion intercalation method [16]. They applied a voltage between cathodic MoS_2 and anodic Li foil using dimethyl carbonate and ethylene carbonate as an electrolyte (current density of 0.05 mA) to exfoliate MoS_2. They applied this electrochemical Li-intercalation and exfoliation process for the synthesis of various TMD nanosheets: MoS_2, WS_2, TiS_2, TaS_2, ZrS_2 and $NbSe_2$. Bulk TMDs coated on a Cu foil were used as cathode and Li foil as an anode. Subsequently, intercalation was performed and the nanosheets were dispersed via sonication in water. However, this Li intercalation method has few drawbacks like the complete removal of Li that causes a doping effect, and also the additional charges in the lithium ions that transforms the 2H phase into 1T phase, which is unfavorable for semiconducting applications.

1.4.2 Bottom-Up Methods

In order to integrate TMDs effectively into electronic devices, it is obligatory to achieve a controlled layer (single to few layers), enhanced-quality (reduced defects, grain boundaries) and scalable crystal growth. While the top-down approach has limitations in meeting these requirements, exploration of other methods with a bottom-up approach became crucial. In the bottom-up approach, atomic/molecular precursors undergo direct chemical reactions to form nanomaterials and this involves methods like physical vapor deposition (PVD), chemical vapor deposition (CVD) and solution chemical process.

1.4.2.1 Physical Vapor Deposition (PVD)

Physical Vapor Deposition (PVD) is a simple and powerful method for depositing different materials over different substrates (metal, semiconductors and insulators). In this process, atoms or small cluster of atoms are transported from solid source to the substrate in a vacuum chamber, to form a thin film. As time increases, a thin layer is formed on the substrate. The deposition rate mainly depends upon substrate to source distance, system pressure and substrate temperature. The PVD deposition technique is mainly classified into three different types: sputtering, pulse laser deposition (PLD) and molecular beam epitaxy (MBE). In sputtering, the target surface (source) at cathode side is bombarded with positive ions generated from a rare gas discharge. The accelerated ions transfer their momentum to target surface, resulting in ejection of atoms. The substrate for film formation is kept at anode side, in opposite side of the target. For sputtering to take place, the threshold energy should be higher than the surface binding energy of the target atoms. In pulse laser deposition method, a highly concentrated laser strikes a small area of target surface. This results in plume formation above the target, containing energetic ions, neutral atoms and molecules. This reaches the substrate with broad energy distribution. For uniform film formation, the target and the substrate are rotated. Molecular beam epitaxy (MBE) is a layer-by-layer atomic growth by using ultra-high

vacuum (UHV) techniques. In UHV environment, 10^{-10} Torr vacuum is maintained and the atoms travel in nearly collision free path before arriving the substrate, leading to the deposition of high-quality film [17].

1.4.2.2 Chemical Vapor Deposition (CVD)

The chemical vapor deposition (CVD) technique is one of the compatible methods for the fabrication of large area uniform MoS_2 nanostructures. Chemical reactions occur during growth, resulting in the deposition of a thin film over the substrate. At reaction temperature, Mo precursor (like MoO_3, $(NH_4)_2MoS_4$ or Mo) deposits on the substrate followed by sulfurization. Wang *et al.* fabricated a highly crystalline MoS_2 film using MoO_2 microcrystals [18]. MoO_3 powder was first evaporated and reduced by S vapor to form MoO_2, that nucleated on SiO_2-Si substrate. Then annealing was done in presence of S vapor at 850-950˚C for 0.5-6 h using Ar gas. Annealing sulfurizes the MoO_2 microplates, producing MoS_2 in rhomboid shape with different layer numbers and domain size of ~10μm. Using the same precursor but different growth condition, edge–terminated vertically oriented (V-type) few-layer MoS_2 sheets was synthesized [19]. The process involves the vaporization of MoO_3 powder using S at 750 ˚C for 10 min in nitrogen environment, resulting in the growth of V-type MoS_2 film. Further, a new self-limiting CVD technique is developed using $MoCl_5$ and S as precursors [20]. The $MoCl_5$ and S powder were kept in the middle and upstream position of the furnace, respectively with the substrate (SiO_2, sapphire or graphite) kept at downstream. The furnace was raised at 850˚C for 10 min in the presence of Ar environment resulting in the successful growth of monolayer or few-layer MoS_2 films of centimeter size. Here layer number is controlled with the amount of $MoCl_5$ precursor. In another CVD process elemental Mo is used for growing large area single crystal MoS_2 [21]. Firstly, e-beam evaporation is used to deposit a thin layer of Mo metal (50 Å) on the substrate. At high temperature, sulfur vaporizes and reacts with Mo on the substrate

in an inert atmosphere. The obtained film depends upon area coverage of Mo on the substrate and its thickness, reaction temperature, sulfur amount and the type of substrate used.

The above-mentioned CVD synthesis methods require a temperature of 600-800˚C and even greater than 1000 ˚C during sulfurization of Mo film. Such high temperature limits the CVD synthesis process directly on the device substrate. Rather, TMD is transferred from the synthesized substrate to a target substrate, which ultimately adds residues that affect the device performance. Plasma-assisted chemical vapor deposition (PECVD) provides a way to synthesis MoS_2 at a lower growth temperature of 150-300˚C with direct synthesis on an arbitrary substrate, even plastic substrate [22] . Low temperature of 400 ˚C produces uniform few-layer MoS_2 film by employing vapor phase MoO_3 with H_2S plasma on an arbitrary substrate by PECVD. Metal-organic chemical vapor deposition (MOCVD) is another type of CVD that requires organometallic precursors for the deposition of highly crystalline semiconducting thin films. Kang *et al.* reported the growth of MoS_2 using gaseous precursor molybdenum hexacarbonyl ($Mo(CO)_6$) and diethyl sulphide ($(C_2H_5)_2S$) on 4-inch substrate (fused silica or SiO_2-Si) by MOCVD [23]. Growth time of ~26 h at 550 ˚C produces monolayer MoS_2 on the substrate.

1.4.2.3 Solution Chemical Process

It is a bottom-up approach for high yield production of nanomaterials with different morphology. The synthesis mechanism consists of nucleation in solution medium followed by growth, which results in a particular architecture depending upon the growth condition. It is classified into three types: hydrothermal, solvothermal and colloidal synthesis. The colloidal route is carried out in a three-neck round bottom flask in an inert atmosphere at a higher temperature and shorter growth time in comparison to the hydro/solvothermal method. Hydrothermal and solvothermal synthesis are alike in many respects like precursors taken, chemical reactions and autoclave used. But the difference between two is that hydrothermal

synthesis involves the chemical reactions in an aqueous solution while solvothermal synthesis is accomplished in a non-aqueous medium (organic solvent like DMF, pyridine or octylamine). In both of these methods, Mo and S precursors are first made to dissolve in a suitable solvent via stirring or sonication. Then it is made to react at moderate temperature (150-250°C) and high pressure for several hours (10-48 h) in a tightly sealed teflon-lined stainless steel container called autoclave. Finally, after cooling, it is washed and left for overnight drying resulting in few-layer MoS_2 structure. To enhance the purity and crystallinity often it is annealed at high temperature. Synthesized MoS_2 may vary in terms of morphology, phase formed, dimension of particle and crystallinity depending upon the type of precursors chosen and their concentration, growth time, growth temperature and pH value. The 1T and 2H phases are formed relying on the growth temperature. Main challenge with this method is the selectivity and limited usage of Mo and S precursor. Some of the reported precursors for Mo are molybdenum trioxide (MoO_3), molybdenum pentachloride ($MoCl_5$), sodium molybdate (Na_2MoO_4), ammonium heptamolybdate ($(NH_4)_6Mo_7O_{24}$), etc., while S precursors include thiourea (NH_2CSNH_2), L-cysteine ($C_3H_7NO_2S$), dibenzyl disulfide ($C_{14}H_{14}S_2$), potassium thiocyanate (KSCN), thioacetamide (C_2H_5NS), etc. Single precursor for both molybdenum and sulfur used is ammonium tetrathiomolybdate ($(NH_4)_2MoS_4$). Adding sodium hydroxide (NaOH) and HCl maintains the pH value, while some reducing agents like N_2H_4 and $NaBH_4$ are also used. Synthesized MoS_2 may have a variety of morphologies such as nanosheets, nanoflakes, nanoflowers, nanodots, nanorods, nanospheres and core-shell structures, with nanosheets being most popular among all. Ren *et al.* have synthesized monolayer MoS_2 quantum dots via hydrothermal method using Na_2MoO_4 and $C_{14}H_{14}S_2$ as Mo and S precursors, respectively [24]. The reaction was executed at 220°C for 18 h in an autoclave. Chung *et al.* have synthesized MoS_2 nanospheres and nanosheets using the hydrothermal approach with Na_2MoO_4 and L-cysteine as Mo and S source, respectively [25]. After adding HCl drop by drop (till pH < 1),

the reaction is performed at 220℃ for 36 h. Next for synthesizing MoS_2 nanosheets, they used the same procedure, by replacing S precursor (L-cysteine) with thiourea. Another approach of the wet chemical method to be discussed is the colloidal synthesis method. It enables the growth of high crystalline monolayer nanostructures with monodispersity as well as control over the edges. The growth mechanism is associated with the quick nucleation followed by growth. If the precursor's concentration falls below the critical concentration, which is essential for the initiation of nucleation, nucleation ceases after a short duration. Lin *et al.* have designed a colloidal route for the synthesis of MoS_2 quantum dot (QD) [26]. A mixture of $(NH_4)_2MoS_4$, oleic acid (OA), oleyl amine (OLA) and 1-octadecene (ODE) is heated at 120 °C for 2.5 h under continuous stirring to get a homogeneous solution. Later the prepared solution is raised to 250 °C for 3 h, resulting in the formation of MoS_2 QD. The OLA reduces $(NH_4)_2MoS_4$ and also act as stabilizing agent that control the size and property of MoS_2. Zhou *et al.* have described the synthesis of single- and multi-layer MoS_2 nanosheets via controllable colloidal route [27]. They have taken molybdenum (II) acetate dimer ($[Mo(Ac)_2]_2$), stearic acid (SA), oleylamine (OAm) and trioctylphosphine oxide (TOPO) in a three-neck round bottom flask and have raised the temperature at 330 °C under nitrogen flow. Various lateral sizes of MoS_2 can be synthesized ranging from 8-25 nm by changing the concentration ratio of Mo and S precursors while a multi-injection approach can be used for obtaining MoS_2 with different layer number.

1.5 Properties of MoS_2 Nanostructures

1.5.1 Electrical and Electronic Properties

The 2D MoS_2 structure displays unique electrical and electronic properties due to quantum confinement and the transformation of indirect energy bandgap for bulk to direct bandgap for monolayer. The charge carrier mobility of MoS_2 is a crucial parameter for its performance in electronic applications. In 1967, Fivaz and Mooser investigated the room

temperature charge carrier mobility in bulk MoS_2 and reported in the range of 200 to 500 cm^2/Vs [28]. Experiments focused on monolayer MoS_2, indicated the decrease in room temperature mobility to 0.1-10 cm^2/Vs [29, 30]. The primary cause for this decline is attributed to the presence of charge traps at the interface between MoS_2 and the substrate [31]. The electrical constants like activation energy, barrier height and trapped energy state can be calculated from the electrical conductivity measurements. The activation energy (E_a) is determined with the help of Arrhenius equation -

$$\sigma = \sigma_0 \, e^{-\frac{E_a}{kT}} \tag{1.1}$$

where σ is the conductivity and σ_0 is a parameter that depends on the characteristics of the sample (thickness, structure). The mobility of charge carriers in MoS_2 can be affected by factors such as temperature, crystal quality, and the presence of defects. Understanding and controlling these factors are essential for optimizing the electrical properties of MoS_2 in various applications, including field-effect transistors, sensors and optoelectronic devices.

The electronic property of MoS_2 is mainly affected by the crystal structure. Zhao *et al.* have compared the band structure of different crystal phases (1T, 2H and 3R) of MoS_2 in case of bulk, bilayer and monolayer [32]. In the 2H-MoS_2, S atom overlaps along the c-axis implying strong repulsive force. As a result, it leads to weaker overlap of wavefunction leading to the existence of a bandgap i.e., it shows semiconducting behavior. Whereas in 1T and 3R phase of MoS_2, S atom doesn't overlap along the c-axis. That shows existence of strong attractive force, leading to a stronger overlap of wavefunction and causing the non-existence of a bandgap i.e., revealing conducting behavior. Semiconducting behavior can be converted into metallic by phase engineering such as Li intercalation. Electronic structure engineering provides the vision in modulating the band structure with layer number. The indirect-to-direct crossover results from the local shift of valence band (VB) hills and conduction band (CB) valleys in the Brillouin zone. The VB maxima and CB minima coincide at K point for

monolayer MoS_2, showing direct bandgap behavior, featured with a wide bandgap of ~1.8 eV. As the number of layer increases, layer interaction increases resulting in raising of VB hill at the Γ point and down-shifts of CB valley in between Γ and K point, thus making it an indirect bandgap semiconductor with ~1.29 eV in case of bulk [33]. As the number of layer decreases, the bandgap increases due to quantum confinement effect along the c-direction of the crystal.

1.5.2 Mechanical Behavior

The mechanical stability of the sample is another important factor to be considered for application in nanodevices. It involves Young's modulus, bending modulus, yield stress and buckling. The TMDs have relatively low mechanical strength compared to graphene. Bertolazzi *et al.* calculated the stiffness along with the breaking strength of single layer MoS_2 using AFM [34]. They calculated in-plane stiffness of single layer MoS_2 ~180 ± 60 Nm^{-1} and Young's modulus ~270 ± 100 GPa. The average breaking strength was measured to be ~15 ± 3 Nm^{-1} and this breaking was arised at an effective strain of 6 to 11%. Nanoindentation experiments have calculated the yields stress of ~16.5 to 15 Nm^{-1}. The single layer MoS_2 has a greater elastic bending modulus (9.61 eV) compared to graphene (1.4 eV) [35].

1.5.3 Optical Behavior

The optical property of a material defines how the material interacts with light and is crucial in industry and scientific work. Investigating optical transmittance proves beneficial for innovative transparent electronics applications that demand materials possessing both high optical transparency and electrical conductivity. An optical transmittance of up to 95% was noted in the single layer MoS_2 film, and this value declined as the film thickness increased [36]. Penetration depth of a particular wavelength of light in the material before it gets completely absorbed is given by the absorption coefficient. Monolayer and multilayer MoS_2 have a high absorption coefficient (α) in the visible region. Penetration of light of a certain

wavelength through a material is defined by the extinction coefficient (k). In case of monolayer MoS_2, k peaks at ~450 nm, i.e., most monolayer MoS_2 absorbs maximum of this particular wavelength of light and for $\lambda > 500$ nm, k has very less values showing the transparency in that range. At ~400 nm, multilayer MoS_2 shows larger peak than monolayer, signifying that at this value of λ, multilayer absorbs more light than monolayer. The relation between extinction coefficient (k) and absorption coefficient (α) is given by [37]-

$$k = \frac{\alpha\lambda}{4\Pi} \tag{1.2}$$

where λ is the wavelength of light. Another unique feature of MoS_2 is the formation of a negative trion on illumination. It is a quasiparticle comprising of an exciton and an electron. This phenomenon is limited for monolayer MoS_2 because all other direct bandgap semiconductors normally form excitons. Trions are formed as a result of valley and spin polarized holes and exhibits large binding energy (20 meV), produced at room temperature [38]. It has a short life, long transport channel and less mobility. Thus, it plants the base for excitonic and spintronic devices. Another important optical property is the anisotropy that stands out as a fundamental physical property in the realm of emerging 2D materials. When incident light interacts with 2D materials, the alteration of either the intensity or the phase of the incident light occurs due to the linear and nonlinear optical responses of these materials. The anisotropic study can be scrutinized by analysing the periodic changes in the intensity of Raman modes, achieved by varying the polarization of the incident light throughout the measurement. It is influenced by factors such as incident excitation wavelength, and the configuration of polarization setup. This study enables the identification of the symmetries associated with the detected phonon modes. Also, by patterning MoS_2 into nanoribbons (20 nm), high optical anisotropy is observed owing to the anisotropy of light absorption in nanoribbon due to quantum confinement in patterned nanoribbon [39]. This characteristic not only offers rich structural insights but also plays a pivotal role in the design and development

of a wide array of nanoscale devices such as polarization-sensitive photodetectors, phototransistors, linearly polarized pulses generators, optical waveplates, optical switches and interconnects, etc.

1.5.4 Thermal Transport Behavior

In addition to the intriguing optical and electronic properties, the thermal transport characteristics of 2D nanomaterials have also gained significant attention. One of the thermal transport properties is the thermal conductivity, that characterizes the material's ability to conduct heat. The 2D materials offer an excellent platform for investigating fundamental energy carrier transport, offering novel pathways for regulating and managing thermal energy in modern integrated circuits. During operation of these devices, excess heat is generated at high current density due to Joule heating and if not dissipated would lead to rise in local temperature, inducing more phonons. As a result, electron-phonon interaction increases, that ultimately leads to decline of carrier mobility and device failure. Thus, for device application, there is an increasing demand for more effective heat management to minimise the self-heating. It follows Fourier's law, represented as $q = -K\nabla T$, where q signifies heat flux density, K is thermal conductivity and ∇T denotes the temperature gradient [40]. Heat transmission occurs via both electrons and phonons, leading to a composite thermal conductivity, $K = K_p + K_e$, where K_p and K_e represents the phonon and electron contributions, respectively [41]. The highest-ever thermal conductivity is observed in single-layer graphene due to strong in-plane carbon bonding and negligible phonon scattering. Balandin *et al.* calculated the room temperature thermal conductivity of suspended monolayer graphene to be in the range ~ (4.84 to 5.30) × 10^3 $Wm^{-1}K^{-1}$ [42]. In comparison to monolayer graphene, the thermal conductivity of 2D MoS_2 is moderate (34 to 84 $Wm^{-1}K^{-1}$) and are crucial for the design of nanoelectronics and thermoelectric devices [43]. Thermal conductivity is degraded by the presence of defects, edge scattering, and doping. It is also observed that the thermal conductivity of suspended

TMDs is largely quenched when transferred on a substrate due to phonons leaking across the material-substrate interface and interfacial scattering. The defect site in these materials can also reduce the thermal conductivity due to the higher phonon-defect scattering.

The methods for determining thermal conductivity are categorized into two groups: transient and steady state. In transient technique, the measurement is carried out as a function of time and includes methods like 3 Omega (3ω), Time-domain thermos-Reflectance (TDTR) and laser Flash technique. While in steady state technique, the thermal conductivity measurement is performed independent of time and includes optothermal Raman (OTR) technique. The brief description is given below.

(a) Three Omega (3ω) Method

The 3ω technique has been used to measure thermal conductivity of bulk materials and thin layers. Here the sample is fabricated on the substrate and a metallic strip is designed directly on the top of the sample that acts both as a heater and temperature sensor [44]. An alternating current at angular frequency ω causes Joule heating due to which the temperature oscillates with a frequency 2ω across the metallic strip (heater). This alters the electrical resistance of the heater at 2ω, resulting in a small voltage signal across the heater at a frequency 3ω. Consequently, this set of techniques is known as "3 omega" method [45, 46].

(b) Time-domain thermos-Reflectance (TDTR) Method

The TDTR method is a powerful experimental technique used to measure the thermal properties of a wide variety of materials through the change of surface reflectance with temperature. In this technique, a mode-locked laser is split into a pump beam and a probe beam by using a polarizing beam splitter [47]. The pump beam is modulated in a frequency range with electro-optic modulator to heat the sample [48]. Typically, the surface of sample is covered with a metal film, ensuring the absorption of the pump laser at the surface. A delay of the

detection beam with respect to pump light is introduced by a mechanical delay stage and this delayed beam is captured by the photodiode detector. The resulting electrical signal is processed by the lock-in amplifier, producing two outputs: the in-phase (V_{in}) and out-of-phase (V_{out}) voltage. Their ratio ($R = -V_{in}/V_{out}$) gives the measured signal and are fitted to heat transfer model established by Cahill *et al.* in 2004, through which thermal conductivity can be extracted [49].

(c) Laser Flash Method

The laser flash method serves as a relatively fast and easy technique of modest accuracy to measure the thermal diffusivity (α) of various materials. It is related to thermal conductivity (κ), by the following relationship [49, 50]-

$$\alpha = \frac{\kappa}{\rho\, C_p} \tag{1.3}$$

where ρ and C_p are the density and specific heat capacity of the sample. Both the thermal diffusivity and thermal conductivity are important material properties used to define how efficiently a material transfers thermal energy and reacts to temperature shifts. This technique involves the application of a short energy pulse laser to heat one side of the sample, and the subsequent time-dependent temperature rise is measured from the opposite side of the sample [51, 52]. The higher its thermal diffusivity, quicker the energy reaches the backside of the sample.

(d) Optothermal Raman (OTR) technique

Optothermal Raman technique is indeed a steady state method used to directly determine the thermal conductivity of thin film or materials. In this non-contact method, Raman spectra act as an effective 'thermometer' to gauge the thermal conductivity of these materials. In this method, a specific wavelength laser of varying power functions acts as a heat source, creating a localized temperature increase within the material. This temperature elevation leads

to shifts in the Raman modes. Additionally, changes in the Raman modes are observed when the sample is exposed to different temperatures while maintaining a constant laser power. Using the premise that heat disperses radially, the thermal conductivity of 2D materials is then derived by employing suitable models. This technique was first employed by Balandin *et al.* in 2008 to assess the in-plane thermal conductivity of a suspended single-layer graphene [42]. To measure the thermal conductivity (k_s) of supported sample, OTR technique is utilized that involves the temperature and power-dependent Raman analyses.

1.6 Applications of MoS_2 Nanostructures

Owing to its remarkable physical and chemical properties, MoS_2 has demonstrated tremendous potential in various applications such as transistors, photodetectors, logical devices, gas sensors and catalysis. **Figure 1.3** schematically illustrates several key areas of application for MoS_2 nanostructures.

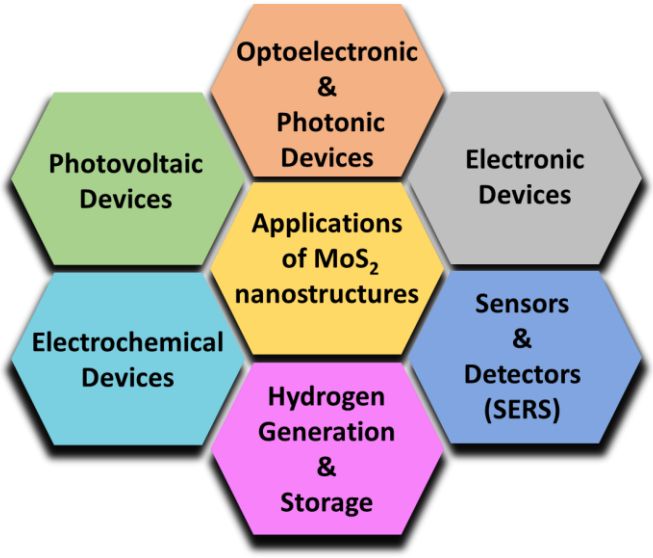

Figure 1.3 *Schematic diagram showing the applications of MoS_2 nanostructures in various fields.*

The porosity and high conductivity of MoS_2, makes them to be used as electrodes for electrochemical applications like supercapacitors, batteries, hydrogen production, etc. [53]. When utilized as a sensitive material, MoS_2 enhances the detection limits for gases like CO,

CO_2, and NO_x [54, 55]. Consequently, the real-world application of wafer-scale MoS_2 is still in its nascent phase. MoS_2 can be used as semiconductors in electronic and optoelectronic devices. Additionally, its good thermal conductivity makes it suitable for thermal management in these devices. MoS_2 can be used as effective substrate for surface enhanced Raman spectroscopy (SERS) technique for optical sensors which can detect ultra-trace concentration of molecules.

1.7 Literature Survey

1.7.1 Literature Survey on Semiconducting Response of MoS_2 Nanostructures

Electronic properties of TMDs are very delicate towards structural perfections and can be tuned by applying external pressure, strain, functionalization, or electromagnetic field. Zhao *et al.* have compared the band structure of different crystal phases (1T, 2H and 3R) of MoS_2 nanosheets in case of bulk, bilayer and monolayer [32]. Kuc *et al.* performed first-principle calculations on the basis of DFT and studied the band structure of MoS_2 with respect to slab thickness going from bulk to monolayer [56]. They showed a notable difference in the bandgap values computed using PBE and PBE0 functionals, concluding better performance with PBE functional with values of 1.8 and 1.2 eV for monolayer and bulk MoS_2, respectively. Bulk structures have bandgap in the range of near infrared. As the layer number decreases to few layers, the blueshift in absorption is observed and the bandgap shifts in the visible range. Photons with energy greater than the direct bandgap is easily absorbed giving absorption and photoluminescence spectra for monolayer MoS_2. Splendiani *et al.* employed DFT with GGA for calculating the electronic band structure of monolayer, bilayer, quadrilayer and bulk MoS_2 [57]. The study demonstrates that the direct bandgap at the K point of the Brillouin zone remains relatively constant with varying layer thickness and the indirect bandgap exhibits a consistent increase as the number of layers decreases. Significantly, in monolayer MoS_2, the indirect transition energy becomes higher, transforming material into direct bandgap

semiconductor. Also, they experimentally measured the variation of bandgap with layer number by performing photoluminescence (PL) and observed the same direct excitonic transition. When moving from bulk to monolayer, the decline in interband relaxation rate results in shift in the electronic band structure and in monolayer, significantly reduced electronic relaxation rate results in enhanced PL. Temperature can be used as another external factor to engineer the bandgap of MoS_2 by thermally inducing change in lattice parameters. Temperature-dependent photoluminescence study can be used to observe thermal response to semiconducting behavior of MoS_2 nanostructures in optoelectronic devices. Xu *et al.* studied the temperature-dependent PL of monolayer MoS_2 synthesized via thermal vapor sulfurization method, and observed the enhanced PL intensity at low temperature [58]. The systematic temperature-dependent PL study and comprehensively analysing the interlayer and spin-orbit coupling effect in CVD grown different layered and differently oriented MoS_2 nanostructures at low temperatures is still missing in the literature.

1.7.2 Literature Survey on Optical Anisotropy Study of MoS_2 Nanostructures

The anisotropic behavior of 2D materials can be investigated by examining the interaction between electrons, phonons and photons during light-matter interaction. Wu *et al.* showed that the isotropic in-plane crystal structure of pristine 1L MoS_2 becomes strongly anisotropic when patterned into nanoribbons [39]. Nam *et al.* investigated the in-plane optical anisotropy of mechanically exfoliated 1T' MoS_2 [59]. They observed that the Raman intensities of peaks at 152, 213, 283, 330 and 404 cm^{-1} strongly vary with angles, exhibiting two and four-fold symmetries. Kim *et al.* reported different anisotropic Raman responses, i.e., more elliptical response of E^1_{2g} mode with increasing layer numbers and the response of A_{1g} mode remains independent with layer number of CVD grown few layers (layer by layer vertical stacked) triangular MoS_2 [60]. Their triangular MoS_2 were having stacking misalignment (interlayer twisting or sliding) between neighbouring layers, which may result in more elliptical polar plot

with increasing layer numbers. Kumar *et al.* reported the anisotropic optical response of CVD and mechanically exfoliated flakes by analyzing the polarization dependence of phonon modes concerning incident photon energy and different flake thickness [61]. Miller *et al.* studied the exciton-phonon coupling in micro-mechanically exfoliated flakes of monolayer MoS_2 using circularly polarized light (488 and 633 nm) in polarization resolved Raman spectroscopy [62]. The anisotropic responses of CVD grown triangular MoS_2 with different layer numbers and excitation sources (resonant and non-resonant) along with differently oriented (horizontal and vertical) MoS_2 films have not been discussed earlier.

1.7.3 Literature Survey on Thermal Transport of MoS_2 Nanostructures

Scientists have effectively utilized the optothermal Raman technique to measure the thermal conductivity of 2D materials. Thripuranthaka *et al.* investigated the linear response of temperature-dependent Raman shifts of few-layer hydrothermally synthesized MoS_2 and WS_2 nanosheets [63]. Sahoo *et al.* predicted the thermal conductivity (via optothermal Raman method) of suspended 11 layer MoS_2 (~52 $Wm^{-1}K^{-1}$), prepared via vapor-phase method [64]. Najmaei *et al.* reported the non-linear temperature response of single to few-layered mechanically exfoliated MoS_2 over SiO_2-Si substrate in the high-temperature region of 300 to 550 K due to major contribution of four phonon process [33]. Jo *et al.* reported the thermal conductivity (via thermal bridge method) of suspended few-layer (4 to 7 layers) MoS_2 to be 44-52 $Wm^{-1}K^{-1}$ [65]. Taube *et al.* investigate the thermal conductivity (via optothermal Raman method) of mechanically exfoliated monolayer MoS_2 supported on SiO_2-Si substrate to be 62.2 $Wm^{-1}K^{-1}$ [66]. They also reported non-linearity of thermal transport in the temperatures range 70 to 350 K [67]. Zhang *et al.* investigated the thermal conductivity of both suspended and supported mono- and bi-layer MoS_2, which was mechanically exfoliated, within the temperature range of 298 to 498 K (84 ± 17 $Wm^{-1}K^{-1}$ for suspended 1L MoS_2, 55 ± 20 $Wm^{-1}K^{-1}$ for supported 1L MoS_2, 77 ± 25 $Wm^{-1}K^{-1}$ for suspended 2L MoS_2, 35 ± 7 $Wm^{-1}K^{-1}$ for

supported 2L MoS_2) [68]. Yuan *et al.* reported the thermal conductivity (via a five-state energy transport state-resolved Raman approach) of micromechanical exfoliated few layer MoS_2 supported on a glass substrate to be decreasing from 60.3 (2.4 nm thick) to 31.0 W m^{-1} K^{-1} (9.2 nm thick) and then increases with increasing thickness [69]. Arrighi *et al.* determined the thermal conductivity (via two-laser Raman scattering thermometry) of suspended, single-crystalline mechanically exfoliated MoS_2 with 5 and 14 nm thickness, to vary between 12-24 $Wm^{-1}K^{-1}$ [70].

Most of the reports concerning the thermal conductivity assessment of MoS_2 have primarily focused on mechanically exfoliated samples, either suspended or supported. However, investigations into CVD-grown supported MoS_2 nanostructures, encompassing different thicknesses, and on thin film CVD-grown MoS_2 supported over conducting substrates, remain notably absent in existing literature. Also, there are limited thermal conductivity reports on vertically oriented MoS_2 nanostructures and needs more exploration. Furthermore, comprehensive studies delving into the non-linear temperature-dependent Raman response of CVD-grown supported MoS_2 are yet to be thoroughly explored in current research. In the present work, we observe the non-linearity in the temperature-dependent Raman spectra and have used the optothermal Raman technique to measure the interfacial thermal conductance and thermal conductivity of different CVD prepared MoS_2 nanostructures.

1.7.4 Literature Survey on SERS Application of MoS_2 Nanostructures

There are only limited research related to the SERS investigation for the detection of biomolecules by utilizing semiconducting 2D MoS_2. Singha *et al.* utilized Au decorated MoS_2 nanoflower (hydrothermally synthesized) as an effective SERS substrate for detecting rhodamine 6G (up to 10^{-12} M concentration) and bilirubin in human serum matrix (up to 10^{-7} M) [71]. Li *et al.* hydrothermally synthesized Fe-doped MoS_2 nanoflowers (Fe-MoS_2 NFs) for detecting bilirubin in serum with LOD of 10^{-8} M [72]. Quan *et al.* reported the SERS biosensor

based on MoS_2@ZnO@Ag SERS substrate for free bilirubin detection in serum (detection limit of 10^{-8} M) [73]. Qiu *et al.* used hierarchical MoS_2-microspheres decorated with cauliflower like Au-nanoparticles as SERS substrate for the detection of rhodamine 6G (up to 10^{-14} M at both 532 and 633 nm), and methylene blue (up to 10^{-14} M at 532 nm and 10^{-15} M at 633 nm) [74]. Limited research in this area requires further more exploration with different morphologies of semiconducting MoS_2 to achieve highest possible detection.

1.8 Scope and Objective of the Present Work

The 2D MoS_2 with different layered and morphology, has aroused scientific breakthrough in technologies, particularly in next-generation photonics, nanoelectronics and optoelectronic applications, owing to their tunable bandgap of ~1.8 eV for monolayer to ~1.29 eV for bulk, large mobility (theoretical values around 410 $cm^2V^{-1}s^{-1}$ and experimental values ranging from 0.1-10 $cm^2V^{-1}s^{-1}$) and a high current on/off ratios of 10^{10} [33, 75, 76]. The device application of these materials requires the knowledge of their thermal, electrical and optical properties associated with electron-phonon interactions. It shows excellent semiconducting nature with tunable bandgap in response to various physical stimuli like temperature, suitable as tunable bandgap material for application in photodetector, solar cell, display technology, transistor etc. The optical anisotropic response of MoS_2 might be useful in designing photonic and optoelectronic devices like polarization-sensitive photodetectors, phototransistors, linearly polarized pulses generators, optical waveplates, optical switches etc. Most of the existing Si based optoelectronic devices have issues with energy loss and hence larger thermal dissipation, which affect their performance. In order to reduce this energy loss and heat dissipation issue, good thermal conducting and direct bandgap semiconductors are needed for the development of next generation devices. Thermal transport properties of MoS_2 can leads to better heat dissipation in electronic devices. Further, the high detection of biomolecules can be achieved

with MoS_2 as a SERS substrates, that may find new insights for practical applications of MoS_2 based SERS biosensors.

The main objectives of the present work are as follows-

- To successfully demonstrate the synthesis of different layer number (1L, 3L and 5L triangular) and different morphologies (horizontally and vertically oriented) MoS_2 nanostructures over different substrates (SiO_2-Si, FTO coated glass and Si) via CVD technique.
- Examining electronic band structure and total DOS for 1 to 6L MoS_2 using DFT calculations. Investigating the effect of layer number, morphology (horizontally/ vertically oriented), substrate dependence on thermal sensitive excitonic response of prepared MoS_2 nanostructures using temperature-dependent photoluminescence spectroscopy.
- Analyzing phonon dispersion curve and phonon density of states for 1 to 6L MoS_2 using density functional perturbation theory (DFPT) calculations. Understanding the effect of layer number, morphology (horizontally/vertically oriented), substrate dependence on anisotropic response of prepared MoS_2 nanostructures using ARPRS study.
- Investigating the effect of layer number, morphology (horizontally/vertically oriented), substrate dependence on thermal transport behavior of prepared MoS_2 nanostructures and identifying their thermal conductivity using optothermal Raman spectroscopy technique.
- Investigating application of different prepared MoS_2 nanostructures as SERS biosensor for the detection of bilirubin and vitamin B_{12} biomolecules.